

We are IntechOpen, the world's leading publisher of Open Access books Built by scientists, for scientists

6,500

Open access books available

176,000

International authors and editors

190M

Downloads

Our authors are among the

154

Countries delivered to

TOP 1%

most cited scientists

12.2%

Contributors from top 500 universities



WEB OF SCIENCE™

Selection of our books indexed in the Book Citation Index
in Web of Science™ Core Collection (BKCI)

Interested in publishing with us?
Contact book.department@intechopen.com

Numbers displayed above are based on latest data collected.
For more information visit www.intechopen.com



Chapter

Nonlinear Robust Control of Trajectory-Following for Autonomous Ground Electric Vehicles

Xianjian Jin and Qikang Wang

Abstract

This chapter proposes a nonlinear robust H -infinity control approach to enhance the trajectory-following capabilities of autonomous ground electric vehicles (AGEV). Given the inherent influence of driving maneuvers and road conditions on vehicle trajectory dynamics, the primary objective is to address the control challenges associated with trajectory-following, including parametric uncertainties, system nonlinearities, and external disturbance. Firstly, taking into account parameter uncertainties associated with the tire's physical limits, the system dynamics of the AGEV and its uncertain vehicle trajectory-following system are modeled and constructed. Subsequently, an augmented system for control-oriented vehicle trajectory-following is developed. Finally, the design of the nonlinear robust H -infinity controller (NRC) for the vehicle trajectory-following system is carried out, which is designed based on the H -infinity performance index and incorporates nonlinear compensation to meet the requirements of the AGEV system. The controller design involves solving a set of linear matrix inequalities derived from quadratic H -infinity performance and Lyapunov stability. To validate the efficacy of the proposed controller, simulations are conducted using a high-fidelity CarSim[®] full-vehicle model in scenarios involving double lane change and serpentine maneuvers. The simulation results demonstrate that the proposed NRC outperforms both the linear quadratic regulator (LQR) controller and the robust H -infinity controller (RHC) in terms of vehicle trajectory-following performance.

Keywords: autonomous vehicles, electric vehicles, trajectory-following, robust control, nonlinear control

1. Introduction

In recent years, the emergence of AGEV has attracted significant attention from the experts and scholars [1, 2]. AGEV technology offers notable benefits such as reducing traffic congestion, minimizing air pollution, and enhancing road safety. One key area of research focus is the application of active front steering (AFS) as a chassis active control technology for AGEV steering systems. AFS employs adaptive steering

gear ratio to improve vehicle stability and active safety. The integration of AFS systems in AGEV provides substantial advantages in terms of driver safety, handling flexibility, and trajectory-following performance for AGEV [3]. The inherent features of AFS, including its rapid response and precise execution, contribute to enhanced active safety and superior trajectory-following performance for AGEV [4, 5].

Extensive researches have been conducted in the literatures on the trajectory-following control of AGEV with AFS system [6–12]. For achieving trajectory-following for AGEV with the AFS system, a controller utilizing the Kalman filter with multi-rate is designed to account for the motor control period and the sampling time of the camera [6]. To address the challenges of the control distribution between steering and the control system for AGEV, a model predictive control (MPC) method is proposed in Ref. [7], which reallocates the braking and steering control based on tire force to precisely follow the desired trajectory. Aiming to enhance steering stability for AGEV, a variable steering ratio AFS controller is developed in Ref. [8], it establishes a mapping between vehicle velocity and steering wheel angle. Based on the linearization of the vehicle's model, the vehicle front steering angle is gained by the AFS system to follow the desired trajectory on slippery roads [9]. Moreover, the advanced steering capabilities of the AFS system have proven valuable in other application areas related to trajectory-following control [10–12].

Despite the success achieved in trajectory-following, there remain challenges in handling system nonlinearity, external disturbances, and uncertain model parameters [13, 14]. For example, researchers have employed various control strategies. Nonlinear model predictive control (NMPC) has been utilized to solve the system nonlinearity and ensure feasibility and convergence [15]. A combination of sliding mode and observer technique is applied to estimate model errors and disturbances for enhancing the system's stability [16]. In the context of Markov jump cyber-physical systems, an adaptive sliding mode control (SMC) framework is proposed to handle safety issues arising from actuator failures and external attacks [17]. For uncertain challenges of robotic arm systems, a switchable neural networks-based SMC framework has been developed to accurately track motion trajectories, which can provide real time control to enhance the stability of the trajectory-following control system by adaptive algorithm [18]. An adaptive fuzzy controller (FC) is developed to address the challenge nonlinear trajectory-following system, and the stability of system is guaranteed by Lyapunov method [19]. Some extensions of FC can be obtained from Refs. [20,21]. Furthermore, active disturbance rejection control is employed to dynamically estimate and offset unmodeled system dynamics and unpredictable external disturbances, it enhances the stability of vehicle trajectory-following system [22]. Speed MPC strategies are proposed to achieve accurate trajectory-following for AGEV [23]. In the milling system, the optimal control and time delay techniques are used to suppress chatter by adaptive extreme value algorithm [24]. To handle the problems of parameter jump in complex nonlinear systems, an adaptive control method with multi-model switching is presented. The least squares technique and some lemmas are also utilized to develop an adaptive control law [25]. For dealing with the system disturbances, a novel optimal control based on iterative techniques is proposed in [26], and it provides the conditions of system asymptotic stability and the H -infinity control. An output feedback-based global adaptive control strategy is proposed to handle system nonlinear time-varying parameters [27]. Moreover, robust control strategies have also been implemented in trajectory-following control, providing benefits in addressing the challenges of system nonlinearity, parameter variation, and external disturbance [28].

Therefore, this chapter develops a novel nonlinear robust control framework for AGEV to address the challenges associated with trajectory-following control, including system nonlinearities, uncertain parameter, and disturbances. Firstly, the dynamics of the AGEV and the trajectory-following system are formulated. Subsequently, taking into account the H -infinity performance criterion, nonlinear system compensation, and aim of the trajectory-following, a nonlinear robust controller for trajectory-following is designed. Then, the robustness and effectiveness of the nonlinear robust controller is validated through MATLAB/Simulink/Carsim Co-simulation platform under two scenes. The following sections are structured as follows: Section 2 introduces vehicle trajectory-following modeling. Section 3 outlines the design of the nonlinear robust controller. Section 4 analyzes and discusses the simulation outcomes, and Section 5 presents the conclusions.

2. Vehicle trajectory-following model

The primary focus of the chapter revolves the trajectory-following problem for AGEV. It is assumed that the suspension is a rigid structure, and under normal driving conditions, the slip angle tends to be small. For facilitating the analysis of vehicle actual motion, the bicycle model is selected:

$$m(\dot{v}_x - v_y\dot{\varphi}) = F_{fy} \sin \delta_f + F_{fx} \cos \delta_f + F_{rx} \quad (1)$$

$$m(\dot{v}_y + v_x\dot{\varphi}) = F_{fy} \cos \delta_f + F_{fx} \sin \delta_f + F_{ry} \quad (2)$$

$$I_z\ddot{\varphi} = l_f(F_{fy} \cos \delta_f + F_{fx} \sin \delta_f) - l_r F_{ry} \quad (3)$$

This model incorporates variables such as mass m , yaw angle φ , lateral velocity v_x and longitudinal velocity v_y , lateral tire forces F_{iy} , longitudinal tire forces F_{ix} , moment of inertia I_z . Specifically, F_y can be expressed:

$$F_y = f_y(\alpha, F_z, s_r, \mu) \quad (4)$$

The computation of α is:

$$\alpha = \tan^{-1}\left(\frac{v_{wy}}{v_{wx}}\right) \quad (5)$$

$$\begin{cases} v_{wfx} = v_x \cos \delta_f + (v_y + l_f\dot{\varphi}) \sin \delta_f \\ v_{wrx} = v_x \cos \delta_f + (v_y - l_r\dot{\varphi}) \sin \delta_f \end{cases} \quad (6)$$

$$\begin{cases} v_{wfy} = v_x \cos \delta_f - (v_y + l_f\dot{\varphi}) \sin \delta_f \\ v_{wry} = v_x \cos \delta_f - (v_y - l_r\dot{\varphi}) \sin \delta_f \end{cases} \quad (7)$$

s_r is defined as follows:

$$s_r = \begin{cases} 1 - \frac{v_{wx}}{rw_w} (rw_w \neq 0, rw_w > v_{wx}) \\ \frac{rw_w}{v_{wx}} - 1 (v_{wx} \neq 0, rw_w < v_{wx}) \end{cases} \quad (8)$$

where the tire's radius and angular velocity are represented by r and w_w , respectively. F_Z is given by the following equation:

$$\begin{cases} F_{Zfl,Zfr} = \frac{l_r mg}{2(l_r + l_f)} \mp \Delta F_1 + \Delta F_2 \\ F_{Zrl,Zrr} = \frac{l_f mg}{2(l_r + l_f)} \mp \Delta F_2 + \Delta F_1 \end{cases} \quad (9)$$

ΔF_1 and ΔF_2 are calculated using specific equations:

$$\begin{cases} \Delta F_1 = \frac{m(\dot{v}_x - v_y w) h_{cog}}{2(l_r + l_f)} \\ \Delta F_2 = \frac{m(\dot{v}_x - v_y w) h_{cog}}{2L_h} + \frac{g m_s h_s}{2L_h} \left(\frac{h_{cog} \xi}{g} - \sin \xi \right) \end{cases} \quad (10)$$

Under the assumption that α is small under driving conditions, the tire forces can be simplified:

$$F_{iy} = N_{ai} \alpha_i, (i = f, r) \quad (11)$$

where N_{ai} is the cornering stiffness. Slip angle α_i can be gained:

$$\alpha_f = \delta_f - \frac{v_y + l_f \dot{\varphi}}{v_x}, \alpha_r = -\frac{v_y + l_r \dot{\varphi}}{v_x} \quad (12)$$

Taking into account the small front wheel angle, we can approximate $\cos \delta_f \approx 1$ and $\sin \delta_f \approx 0$. Additionally, we assume AGEV only moves in the horizontal plane, and it neglects the influence of other effects. Consequently, based on Eqs. (11) and (12), Eqs. (2) and (3) can be rewritten:

$$\ddot{y} = -\frac{N_{af} + N_{ar}}{m v_x} \dot{y} - \left(\frac{l_f N_{af} - l_r N_{ar}}{m v_x} + v_x \right) \dot{\varphi} + w_2 \quad (13)$$

$$\ddot{\varphi} = -\frac{l_f N_{af} - l_r N_{ar}}{I_z v_x} \dot{y} - \frac{l_f^2 N_{af} + l_r^2 N_{ar}}{I_z v_x} \dot{\varphi} + w_4 \quad (14)$$

where w_2 and w_4 represent the model state error.

During the trajectory-following process of the AGEV, it is crucial to consider state information of the vehicle. **Figure 1** depicts the diagram illustrating the trajectory-following process of the AGEV. The current and expected yaw angles are represented by φ and φ_r , respectively. Furthermore, the derivatives of y_e and φ_e can be expressed:

$$\dot{y}_e = v_y - v_x \varphi_e \quad (15)$$

$$\dot{\varphi}_e = \dot{\varphi} - \dot{\varphi}_r = \dot{\varphi} - \chi \dot{s} \quad (16)$$

The derivative information of s can be expressed as:

$$\dot{s} = v_x + v_y \varphi_e \quad (17)$$

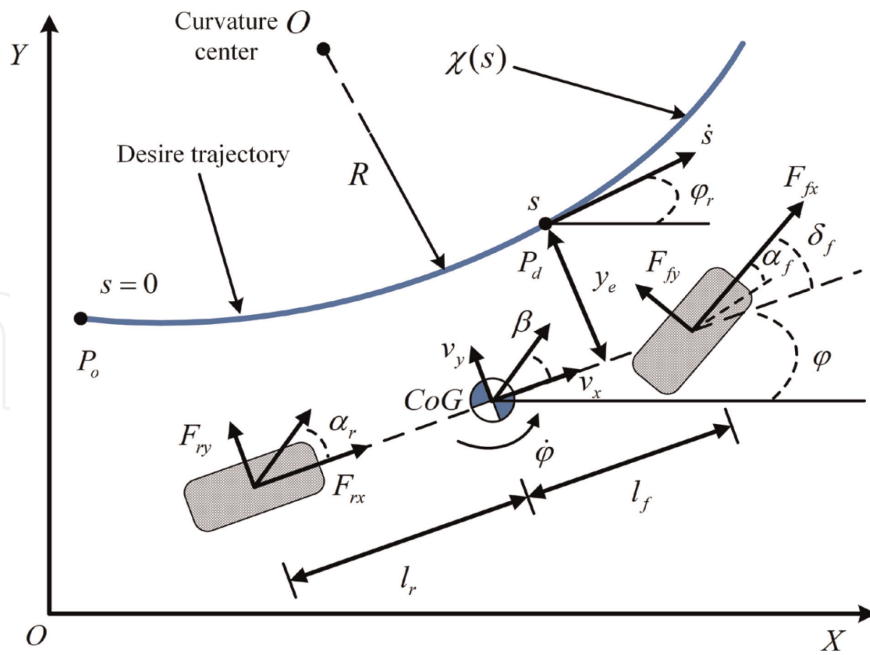


Figure 1.
 The diagram illustrating the trajectory-following process of the AGEV.

$$\ddot{s} = \dot{v}_x + \dot{v}_y \varphi_e + v_y \dot{\varphi}_e \quad (18)$$

By utilizing Eqs. (15)–(18), the derivatives of y_e and φ_e are transformed into Eqs. (19) and (20), respectively.

$$\ddot{y}_e = \dot{v}_y - \dot{v}_x \varphi_e - v_x \dot{\varphi}_e \quad (19)$$

$$\ddot{\varphi}_e = \dot{\zeta} - \dot{\chi} \dot{s} - \chi \ddot{s} \quad (20)$$

The vehicle dynamics mentioned can be reformulated into a state space representation:

$$\dot{x} = Ax + Bu + B_w w \quad (21)$$

$$x = \begin{bmatrix} y_e \\ \dot{y}_e \\ \varphi_e \\ \dot{\varphi}_e \end{bmatrix}, A = \begin{bmatrix} 0 & 1 & 0 & 0 \\ 0 & -\frac{N_{af} + N_{ar}}{m v_x} & \frac{N_{af} + N_{ar}}{m} & -\frac{l_f N_{af} - l_r N_{ar}}{m v_x} \\ 0 & 0 & 0 & 1 \\ 0 & -\frac{l_f N_{af} - l_r N_{ar}}{I_z v_x} & \frac{l_f N_{af} - l_r N_{ar}}{I_z} & -\frac{l_f^2 N_{af} + l_r^2 N_{ar}}{I_z v_x} \end{bmatrix}, B_w = \begin{bmatrix} 0 \\ 1 \\ 0 \\ 1 \end{bmatrix}^T$$

$$B = \begin{bmatrix} 0 & \frac{N_{af}}{m} & 0 & \frac{l_f N_{af}}{I_z} \end{bmatrix}^T$$

The correlation between front wheel angle δ_f and steering wheel angle δ_a can be represented:

$$\delta_a = \tau_f \delta_f \quad (22)$$

where τ_f is the gear ratio.

As AGEV navigate through complex and dynamic road conditions, N_i ($i = \alpha f, \alpha r$) vary and remain within certain bounds. This variation can be addressed in the following manner:

$$N_i = \bar{N}_i + n_i \tilde{N}_i, |n_i| < 1 (i = \alpha f, \alpha r) \quad (23)$$

$$\bar{N}_{\alpha z} = \frac{N_{\alpha z \min} + N_{\alpha z \max}}{2} (z = f, r) \quad (24)$$

$$\tilde{N}_{\alpha z} = \frac{N_{\alpha z \max} - N_{\alpha z \min}}{2} (z = f, r) \quad (25)$$

The maximum and minimum values of N_i ($i = \alpha f, \alpha r$) are denoted as $N_{i \max}$ and $N_{i \min}$, respectively. The time-varying parameters n_i of the system satisfy the condition $|n_i| \leq 1 (i = \alpha f, \alpha r)$.

The system model (21) can be modified as follows:

$$\dot{x} = A_d x + B_d u + B_w w \quad (26)$$

The arguments in the equation have the following significance:

$$A_d = \bar{A}_d + \Delta A, B_d = \bar{B}_d + \Delta B, [\Delta A \quad \Delta B] = H_d F_d [E_A \quad E_B], |F_d| \leq 1 \bar{A}_d =$$

$$\begin{bmatrix} 0 & 1 & 0 & 0 \\ 0 & -\frac{\bar{N}_{\alpha f} + \bar{N}_{\alpha r}}{m v_x} & \frac{\bar{N}_{\alpha f} + \bar{N}_{\alpha r}}{m} & -\frac{l_f \bar{N}_{\alpha f} - l_r \bar{N}_{\alpha r}}{I_z} \\ 0 & 0 & 0 & 1 \\ 0 & -\frac{l_f \bar{N}_{\alpha f} - l_r \bar{N}_{\alpha r}}{I_z v_x} & \frac{l_f \bar{N}_{\alpha f} - l_r \bar{N}_{\alpha r}}{I_z} & -\frac{l_f^2 \bar{N}_{\alpha f} + l_r^2 \bar{N}_{\alpha r}}{I_z v_x} \end{bmatrix}, \bar{B}_d = \begin{bmatrix} 0 \\ \frac{\bar{N}_{\alpha f}}{m} \\ 0 \\ \frac{l_f \bar{N}_{\alpha f}}{I_z} \end{bmatrix}$$

$$E_A = \begin{bmatrix} 0 & -\frac{1}{m v_x} & \frac{1}{m} & -\frac{l_f}{m v_x} \\ 0 & -\frac{1}{m v_x} & \frac{1}{m} & \frac{l_r}{m v_x} \\ 0 & -\frac{l_f}{I_z v_x} & \frac{l_f}{I_z} & -\frac{l_f^2}{I_z v_x} \\ 0 & \frac{l_r}{I_z v_x} & -\frac{l_r}{I_z} & -\frac{l_r^2}{I_z v_x} \end{bmatrix}, H_d = \begin{bmatrix} 0 & 0 & 0 & 0 \\ \tilde{N}_{\alpha f} & \tilde{N}_{\alpha r} & 0 & 0 \\ 0 & 0 & 0 & 0 \\ 0 & 0 & \tilde{N}_{\alpha f} & \tilde{N}_{\alpha r} \end{bmatrix}, E_B = \begin{bmatrix} \frac{1}{m} \\ 0 \\ \frac{l_f}{I_z} \\ 0 \end{bmatrix}$$

3. The design of nonlinear robust controller

3.1 Robust feedback control design

To achieve the desired trajectory tracking, an error function is defined and a robust linear feedback gain is designed as follows:

$$J_s = \int_0^{\infty} q_1 y_e^2 + q_2 \dot{y}_e^2 + q_3 \varphi_e^2 + q_4 \dot{\varphi}_e^2 + q_4 \delta^2 dt \quad (27)$$

where the letter symbols in the equation hold the following meanings:

$$y_e = y_a - y_d, \dot{y}_e = v_y - v_x \varphi_e, \varphi_e = \varphi - \varphi_r, \dot{\varphi}_e = \dot{\varphi} - \chi \dot{s}$$

The equation presented above can be expressed as follows:

$$\begin{aligned} J &= \int_0^{\infty} \left[(\bar{C}_1 x + \bar{D}_{11} w)^T U (\bar{C}_1 x + \bar{D}_{11} w) + u^T V u \right] dt \\ &= \int_0^{\infty} \left[\left(U^{\frac{1}{2}} \bar{C}_1 x + U^{\frac{1}{2}} \bar{D}_{11} w \right)^T \left(U^{\frac{1}{2}} \bar{C}_1 x + U^{\frac{1}{2}} \bar{D}_{11} w \right) + \int_0^{\infty} \left(V^{\frac{1}{2}} u \right)^T \left(V^{\frac{1}{2}} u \right) dt \right] dt \end{aligned} \quad (28)$$

The arguments in the equation hold the following significance:

$$\bar{C}_1 = \begin{bmatrix} 1 & 0 & 0 & 0 \\ 0 & 1 & 0 & 0 \\ 0 & 0 & 1 & 0 \\ 0 & 0 & 0 & 1 \end{bmatrix}, \bar{D}_{11} = 1, U = \begin{bmatrix} q_1 & 0 & 0 & 0 \\ 0 & q_2 & 0 & 0 \\ 0 & 0 & q_3 & 0 \\ 0 & 0 & 0 & q_4 \end{bmatrix}, V = q_5$$

The control output z can be obtained:

$$z = C_1 x + D_{11} w + D_{12} u \quad (29)$$

where:

$$C_1 = \begin{bmatrix} U^{\frac{1}{2}} \bar{C}_1 \\ 0 \end{bmatrix}, D_{11} = \begin{bmatrix} U^{\frac{1}{2}} \bar{D}_{11} \\ 0 \end{bmatrix}, D_{12} = \begin{bmatrix} 0 \\ V^{\frac{1}{2}} \end{bmatrix}$$

The error cost function J is related to the control output z in the following manner:

$$J = \|z\|_2^2 \quad (30)$$

By utilizing the aforementioned system model (26) and the control output of the system (29), the problem of trajectory-following can be reformulated as a standard H -infinity control problem.

$$\begin{cases} \dot{x} = A_d x + B_w w + B_d u \\ z = C_1 x + D_{11} w + D_{12} u \end{cases} \quad (31)$$

In accordance with H_{∞} control theory, the aim of this trajectory-following system is to devise a controller $u_L = Kx$ that satisfy the requirements of trajectory-following for AGEV.

By utilizing Eq. (31) and the state feedback controller $u_L = Kx$, it can derive the vehicle trajectory-following system.

$$\begin{cases} \dot{x} = A_s x + B_s w \\ z = C_s x + D_s w \end{cases} \quad (32)$$

where:

$$A_s = \bar{A}_d + \bar{B}_d K + H_d F_d (E_A + E_B K), B_s = B_w, C_s = C_1 + D_{12} K, D_s = D_{11}$$

Within this investigation, w is regarded as an external disturbance affecting the system. The representation of the system's transfer function (32) can be formulated as follows:

$$T(s) = C_s (sI - A_s) B_s + D_s \quad (33)$$

$w(t)$ and $z(t)$ are presented:

$$\|\Xi\|_2^2 = \int_0^{+\infty} \Xi^T(t) \Xi(t) dt, \Xi = w, z \quad (34)$$

The definition of the H -infinity norm is given by:

$$\|T(s)\|_\infty = \sup_{w \neq 0} \frac{\|z\|_2}{\|w\|_2} \quad (35)$$

In other words, the H -infinity norm represents system maximum singular value. The object of the H -infinity is to find K that satisfies the desired following performance while constraining the impact of disturbances on the output to a specific level. Hence, the subsequent H -infinity performance index is chosen:

$$\frac{\int_0^\infty z^T(t) z(t) dt}{\gamma^2} < \int_0^\infty w^T(t) w(t) dt \quad (36)$$

In order to demonstrate the stability and H_∞ performance of the system (33), several lemmas will be presented.

Lemma 1 [14, 21]: Given matrix $P = \begin{bmatrix} P_{11} & P_{12} \\ P_{21} & P_{22} \end{bmatrix}$, where $P = P^T$, the conditions (37)–(39) are equivalent:

$$P < 0 \quad (37)$$

$$P_{11} < 0, P_{22} - P_{12}^T P_{11}^{-1} P_{12} < 0 \quad (38)$$

$$P_{22} < 0, P_{11} - P_{12} P_{22}^{-1} P_{12}^T < 0 \quad (39)$$

Lemma 2 [26, 27]: Let F be an appropriately dimensioned matrix such that $P = P^T$. Suppose M and N are symmetric real matrices, and $F^T F \leq 1$. Under these conditions, the following inequality holds:

$$P + M F N + N^T F^T M^T < 0 \quad (40)$$

The existence of a positive value $\alpha > 0$ satisfying the following inequality is both sufficient and necessary conditions:

$$P + \alpha M M^T + \alpha^{-1} N^T N < 0 \quad (41)$$

The H -infinity control gain K for trajectory-following system (33) can be obtained by applying the developed Theorem 1.

Theorem 1: In order to ensure both the stability and H_∞ performance of the system, certain conditions need to be satisfied. These conditions involve the existence of symmetric matrices $Y > 0$, $X > 0$, and positive values γ and η , which satisfy the inequality (42). Furthermore, there should exist a H_∞ control gain K for the system that fulfills the following equation.

$$\begin{bmatrix} \text{syms}(\bar{A}_d Y + \bar{B}_d X) & B_w & \Upsilon_1 & \varepsilon H_d & \Upsilon_2 \\ * & -\gamma I & D_{11}^T & 0 & 0 \\ * & * & -\gamma I & 0 & 0 \\ * & * & * & -\eta I & 0 \\ * & * & * & * & -\eta I \end{bmatrix} < 0 \quad (42)$$

where:

$$\text{syms}(\ast) = \ast + \ast^T, \Upsilon_1 = Y C_1^T + X^T D_{12}^T, \Upsilon_2 = Y E_A^T + X^T E_B^T$$

Proof: The condition of stability and H_∞ performance for system (32) is that there exists a symmetric matrix $U > 0$ and value γ that satisfies:

$$\begin{bmatrix} U A_s + A_s^T U & U B_s & C_s^T \\ * & -\gamma I & D_s^T \\ * & * & -\gamma I \end{bmatrix} < 0 \quad (43)$$

Inequation (43) can be written:

$$\begin{bmatrix} \text{syms}(U(\bar{A}_d + \bar{B}_d K) + U H_d F_d (E_A + E_B K)) & U B_w & (C_1 + D_{12} K)^T \\ * & -\gamma I & D_{11}^T \\ * & * & -\gamma I \end{bmatrix} < 0 \quad (44)$$

Inequation (44) further rewrite:

$$\begin{bmatrix} \text{syms}(U(\bar{A}_d + \bar{B}_d K)) & U B_w & C_s^T \\ * & -\gamma I & D_{11}^T \\ * & * & -\gamma I \end{bmatrix} + \begin{bmatrix} \text{syms}(U H_d F_d (E_A + E_B K)) & 0 & 0 \\ * & 0 & 0 \\ * & * & 0 \end{bmatrix} < 0 \quad (45)$$

Inequation (45) is equivalent to:

$$\begin{bmatrix} \text{syms}(U(\bar{A}_d + \bar{B}_d K)) & U B_w & C_s^T \\ * & -\gamma I & D_{11}^T \\ * & * & -\gamma I \end{bmatrix} + \begin{bmatrix} U H_d \\ 0 \\ 0 \end{bmatrix} F_d [(E_A + E_B K) \quad 0 \quad 0] \\ + \begin{bmatrix} (E_A + E_B K)^T \\ 0 \\ 0 \end{bmatrix} F_d^T [(U H_d)^T \quad 0 \quad 0] < 0 \quad (46)$$

Assume that:

$$\bar{H}_d = [UH_d \ 0 \ 0]^T, \bar{F}_d = F_d \quad (47)$$

$$\bar{E}_{AB} = [(E_A + E_B K) \ 0 \ 0] \quad (48)$$

$$\varpi = \begin{bmatrix} \text{syms}(U(\bar{A}_d + \bar{B}_d K)) & UB_w & C_{cl}^T \\ * & -\gamma I & D_{11}T \\ * & * & -\gamma I \end{bmatrix} \quad (49)$$

Inequation (46) can be written as the following conditions:

$$\varpi + \bar{H}_d \bar{F}_d \bar{E}_{AB} + \bar{E}_{AB}^T \bar{F}_d^T \bar{H}_d^T < 0 \quad (50)$$

Based on lemma 2, there exists $\eta > 0$ satisfy:

$$\varpi + \eta \bar{H}_d \bar{H}_d^T + \eta^{-1} \bar{E}_{AB} \bar{E}_{AB}^T < 0 \quad (51)$$

Inequation (51) can be gained from Lemma 1.

$$\begin{bmatrix} \varpi & \bar{H}_d & \bar{E}_{AB}^T \\ * & -\eta^{-1}I & 0 \\ * & * & -\eta I \end{bmatrix} < 0 \quad (52)$$

Expand the inequality (52), according to the property of linear matrix inequality and $\text{diag}\{U^{-1}, I, I, \eta, I\}$. Let $Y = U^{-1}$, $KY = X$, Theorem 1 can be obtained.

3.2 Nonlinear robust control design

Subsequently, in order to enhance system's rapid response and minimize overshoot, the design of the nonlinear compensation feedback control part will be formulated as follows:

$$u_{nla} = \rho(r, h) B^T Q x \quad (53)$$

Here, the nonlinear compensation function $\rho(r, h)$ is introduced, and it depends on the error state x , the reference value r and actual value h . Q can be obtained:

$$A_s^T Q + Q A_s + W = 0 \quad (54)$$

$$W = 100^l \cdot I \quad (55)$$

where l is adjustable value.

The nonlinear compensation part is as follows:

$$\rho(r, h) = -\beta \frac{1}{1 - e^{-1}} \left(e^{-\alpha \left| 1 - \frac{h-h_0}{r-h_0} \right|} - e^{-1} \right) \quad (56)$$

where α and β are positive adjustable parameters.

By integrating the linear part and the nonlinear part, the actuator's output is ultimately derived in the subsequent expression (57). The utilization of linear feedback part facilitates swifter system response within the trajectory-following, while concurrently, the nonlinear compensation part attains stable output and diminishes system overshoot.

$$u_{final} = Kx + \rho(r, h)B^T Qx \quad (57)$$

Based on the aforementioned nonlinear compensation part, and taking into account the saturation of the system's actuator output, the nonlinear robust control system model can be reformulated in the subsequent manner.

$$\begin{cases} \dot{x} = A_d x + B_w w + B_d \text{sat}(u_{final}) \\ z = C_1 x + D_{11} w + D_{12} \text{sat}(u_{final}) \end{cases} \quad (58)$$

$$\text{sat}(u_{final}) = \begin{cases} u_{\max}, & u_{final} > u_{\max} \\ Kx + \rho(r, h)B^T Qx, & |u_{final}| < u_{\max} \\ -u_{\max}, & u_{final} < -u_{\max} \end{cases} \quad (59)$$

Taking into account the saturation of the front wheel angle, the actual expression for the nonlinear compensation can be represented as follows:

$$u_{nla} = \text{sat}(u) - Kx \quad (60)$$

Based on the aforementioned conditions, the expression for u_{nla} can be formulated as follows.

$$0 < |u_{nla}| < \rho(r, h)B^T Qx \quad (61)$$

Subsequently, the impact of the nonlinear compensation on H -infinity performance and stability of the system will be demonstrated.

Proof: The Lyapunov functional V is defined as follows:

$$V = x^T Sx \quad (62)$$

$$\begin{aligned} \dot{V} &= \dot{x}^T Sx + x^T \dot{S}x = (\bar{A}x + \bar{R}x + B_w w)^T Sx + x^T S(\bar{A}x + \bar{R}x + B_w w) \\ &= x^T \bar{A}^T Sx + x^T \bar{R}^T Sx + w^T B_w^T Sx + x^T S\bar{A}x + x^T S\bar{R}x + x^T S B_w w \\ &= x^T (\bar{A}^T S + S\bar{A})x + x^T (\bar{R}^T S + S\bar{R})x + w^T B_w^T Sx + x^T S B_w w \end{aligned} \quad (63)$$

where:

$$\bar{A} = A_d + B_d K, \bar{R} = B_d u_{nla}$$

When $w = 0$:

$$\dot{V} = x^T (\bar{A}^T S + S\bar{A})x + x^T (\bar{R}^T S + S\bar{R})x \quad (64)$$

Assuming that:

$$V_1 = x^T (\bar{A}^T S + S \bar{A}) x \quad (65)$$

It can be inferred that $V_1 > 0$.

Assuming that

$$V_2 = x^T (\bar{R}^T S + S \bar{R}) x = 2x^T S B (\text{sat}(Kx + \rho B^T S x) - Kx) = 2m(\text{sat}(n + \rho m) - n) \quad (66)$$

where:

$$m = x^T S B, n = Kx$$

When actuator output is not saturated:

$$|\text{sat}(n + \rho m)| < u_{\max} \quad (67)$$

At this time:

$$V_2 = 2m(\text{sat}(n + \rho m) - n) = 2\rho m^2 < = 0 \quad (68)$$

Therefore:

$$\dot{V} = V_1 + V_2 = x^T (\bar{A}^T S + S \bar{A}) x + 2m(\text{sat}(n + \rho m) - n) < = x^T (\bar{A}^T S + S \bar{A}) x < 0 \quad (69)$$

When actuator output is saturated:

$$|\text{sat}(n + \rho m)| \geq u_{\max} \quad (70)$$

Suppose that j is saturated and $\rho m = 0$, the system is asymptotically stable.

When j is not subjected to saturation, the output can take on the following two forms:

$$\begin{cases} m < 0, \text{sat}(n + \rho m) - n \geq 0, & \text{When } n + \rho m \geq u_{\max} \text{ and } n > 0 \\ m > 0, \text{sat}(n + \rho m) - n \leq 0, & \text{When } n + \rho m \leq -u_{\max} \text{ and } n < 0 \end{cases} \quad (71)$$

It can be observed from the inequality condition (71): $V_2 = 2m(\text{sat}(n + \rho m) - n) < = 0$ (72)

Thus:

$$\dot{V} = V_1 + V_2 = x^T (\bar{A}^T S + S \bar{A}) x + 2m(\text{sat}(n + \rho m) - n) < = x^T (\bar{A}^T S + S \bar{A}) x < 0 \quad (72)$$

Thus, the system with a nonlinear compensation function is asymptotically stable without interference.

Next, the stability and H -infinity performance of the system with a nonlinear compensation function under external disturbances will be demonstrated.

Let initially establish a cost function J_f :

$$J_f = \dot{V} + z^T z - \gamma^2 w^T w \quad (73)$$

Since the system exhibits asymptotic stability, then if the H -infinity satisfies the following inequality:

$$\|z\|^2 < \gamma^2 \|w\|^2 \quad (74)$$

Then, inequality (76) exists

$$J_f = \dot{V} + z^T z - \gamma^2 w^T w < 0 \quad (75)$$

The above inequality (76) can be further rewritten:

$$J_f = \begin{bmatrix} x \\ w \end{bmatrix}^T \left(\begin{bmatrix} \bar{A}^T S + S\bar{A} + 2S\bar{R} & SB_w \\ * & 0 \end{bmatrix} + \begin{bmatrix} C^T C & C^T D \\ * & D^T D \end{bmatrix} + \begin{bmatrix} 0 & 0 \\ * & \gamma^2 \end{bmatrix} \right) \begin{bmatrix} x \\ w \end{bmatrix} \quad (76)$$

Based on inequality (77) and the characteristics of quadratic form, it can establish the following inequality:

$$\Psi = \begin{bmatrix} \bar{A}^T S + S\bar{A} + 2S\bar{R} & SB_w \\ * & 0 \end{bmatrix} + \begin{bmatrix} C^T C & C^T D \\ * & D^T D \end{bmatrix} + \begin{bmatrix} 0 & 0 \\ * & \gamma^2 \end{bmatrix} \quad (77)$$

Based on Lemma 1:

$$\Psi = \begin{bmatrix} \bar{A}^T S + S\bar{A} + 2S\bar{R} & SB_w & C^T \\ * & \gamma^2 I & D^T \\ * & * & -I \end{bmatrix} \quad (78)$$

Let $U = S$, Eq. (79) is negative from Theorem 1, inequality (66), (68), and (72). Thus, the stability and H -infinity performance of system with nonlinear compensation function is proved.

4. Simulation and analysis

This section simulates and validates the proposed nonlinear robust H -infinity state-feedback controller on the MATLAB/Simulink-Carsim[®]. The simulation framework is implemented using MATLAB/Simulink, while the high-fidelity dynamics model for AGEV trajectory-following is provided by CarSim[®] software. **Figure 2** illustrates the simulation flowchart, and **Table 1** defines the key parameters of AGEV.

The simulation scenarios include double lane change (DLC) road and serpentine road scenes, with a constant forward speed of 54 km/h. These road scenes are chosen to evaluate the controller's robust following ability and steady-state response

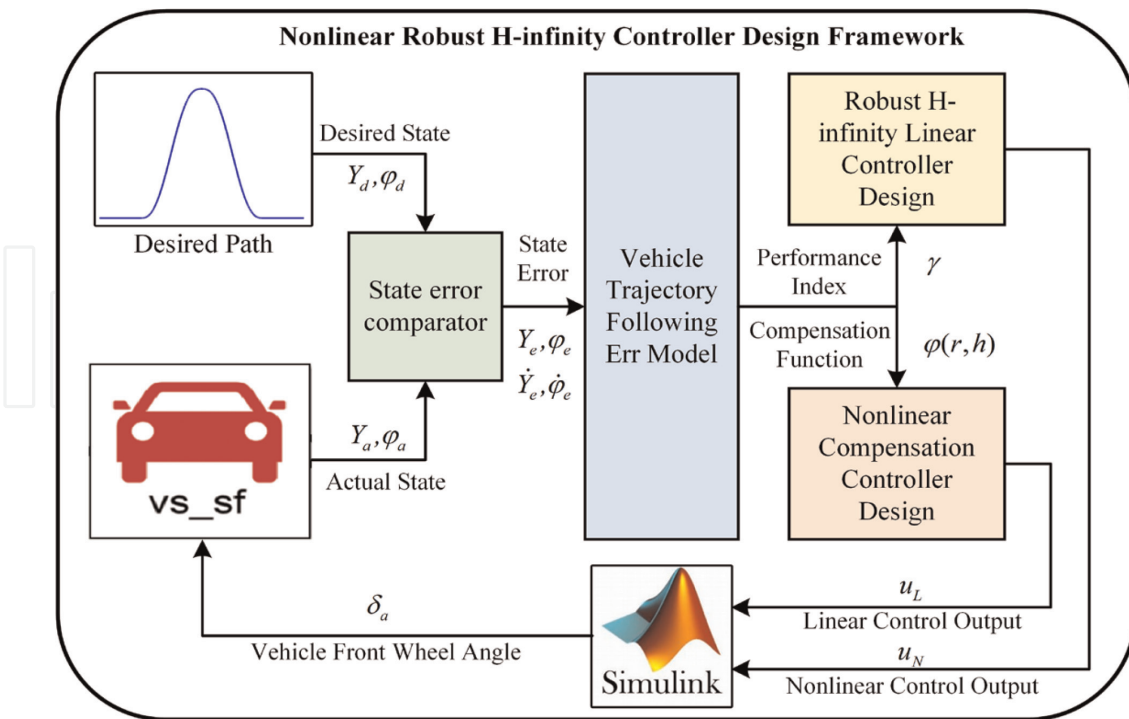


Figure 2. Flowchart of system simulation framework.

Parameter	Scale	Unit	Parameter	Scale	Unit
m	1413	kg	I_z	1536.7	kg·m ²
N_{cf}	[97,996,119,772]	N/rad	N_{cr}	[79,351,96,985]	N/rad
l_f	1.015	m	l_z	0.54	m
l_r	1.895	m	r	0.325	m

Table 1. The key parameters of the vehicle.

performance. For comparison purposes, the performance of the proposed controller is also compared with that of the LQR and RHC controllers.

4.1 Double lane change scene

The simulation results for double lane change (DLC) are presented in **Figures 3–9**, depicting global trajectories, lateral errors, road curvature, front wheel angle, yaw, yaw error, linear angle, and nonlinear compensation part. **Figures 3** and **4** show the global trajectories and lateral errors obtained from three controllers during DLC scenario. All three controllers exhibit satisfactory tracking performance. The maximum of the lateral error for LQR controller is approximately 0.4 m, while for the RHC controller it is around 0.24 m. Notably, the NRC controller achieves a smaller maximum lateral error compared to the other two controllers, indicating its superior tracking performance. Furthermore, **Figure 3** demonstrates that NRC maintains exceptional system response within the range of 45 to 55 meters, further it highlights NRC has ability to enhance the transient performance of the system.

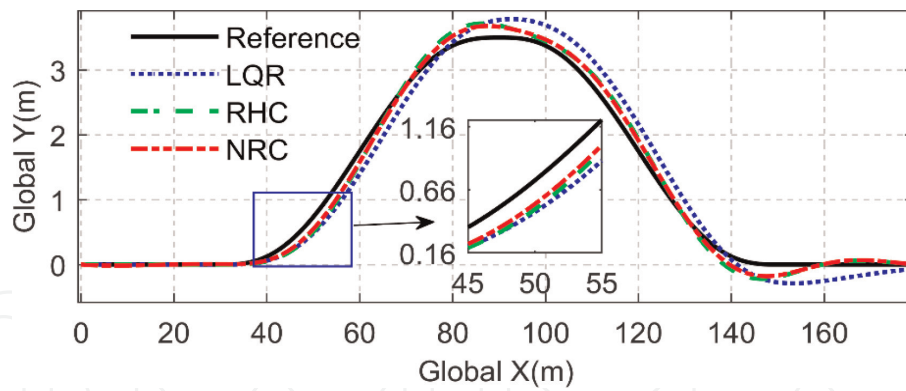


Figure 3.
 Global trajectories of three controllers under DLC scene.

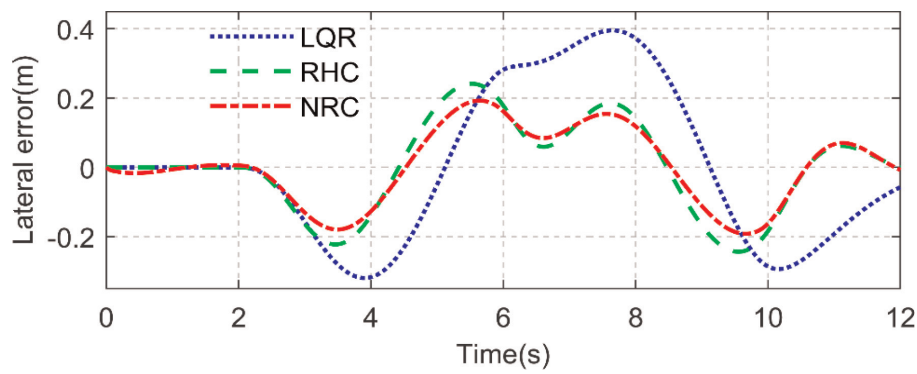


Figure 4.
 Lateral errors of three controllers under DLC scene.

The road curvature and front wheel angle for AGEV during DLC scene are illustrated in **Figures 5** and **6**. **Figure 6** indicates that the front wheel angle of the NRC controller consistently falls between that of the LQR and RHC controllers. It is attributed to the fact that a too small front wheel angle would result in a slow system response, while a too large front wheel angle would lead to significant overshoot. The NRC controller incorporates a linear feedback part to enhance the system response and a nonlinear compensation part to mitigate excessive overshoot. As a result, the NRC controller demonstrates excellent trajectory-following capabilities.

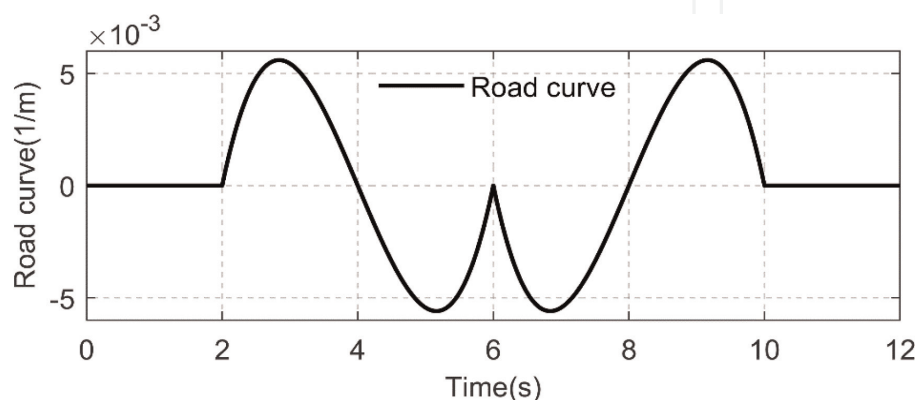


Figure 5.
 Curvature of road under DLC scene.

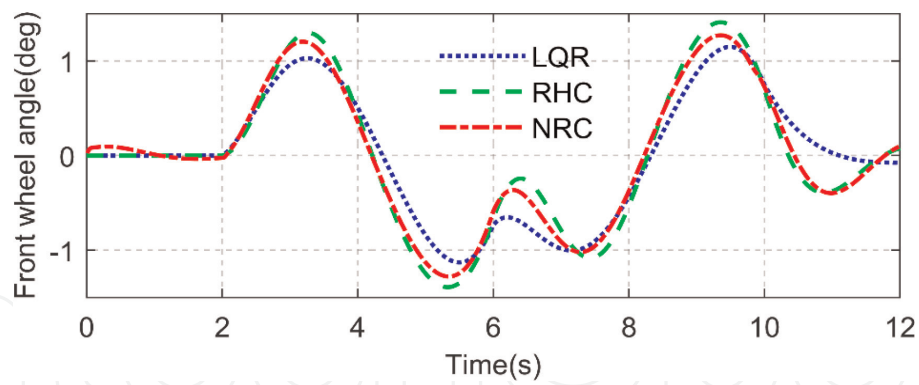


Figure 6.
Front wheel angle of three controllers under DLC scene.

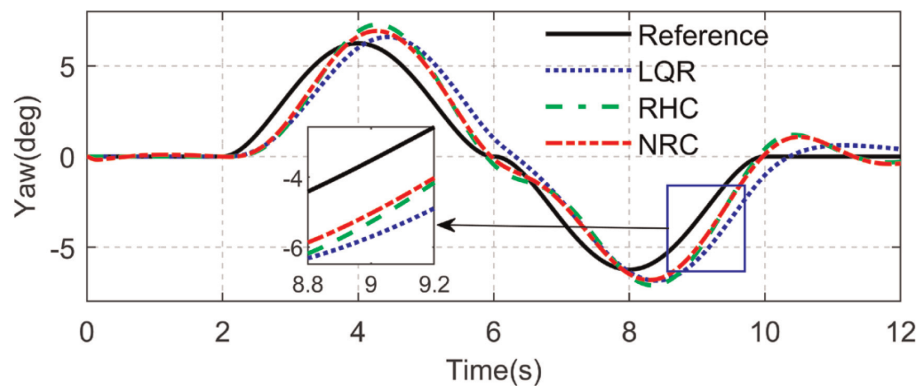


Figure 7.
Yaw of three controllers under DLC scene.

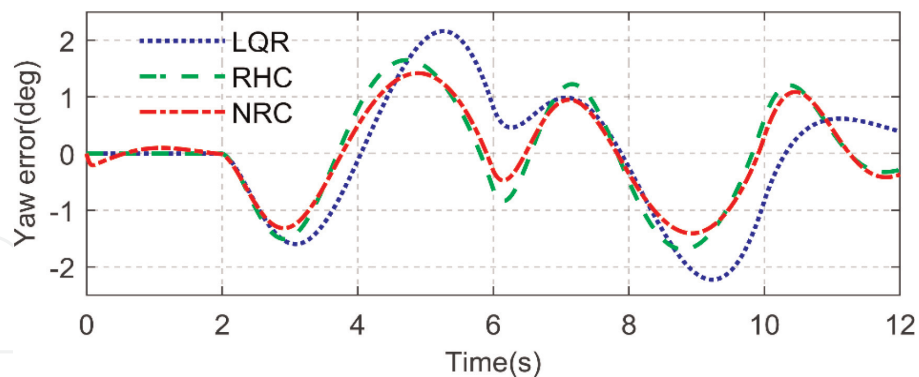


Figure 8.
Yaw error of three controllers under DLC scene.

Figures 7 and 8 depict the yaw and yaw error of the NRC controller, and the NRC controller exhibits smaller yaw error and excellent trajectory-following capabilities compared to the RHC and LQR controllers. The angle of the linear feedback and nonlinear compensation of the NRC controller are illustrated in **Figure 9**. Notably, while the lateral error is smaller, the system nonlinear part of the NRC controller is significant. Conversely, as the vehicle lateral error increases, the system nonlinear part gradually decreases. It aligns with the design intention of the NRC controller, wherein the system exhibits fast response under increasing error scenes and small overshoot when the error is minimal.

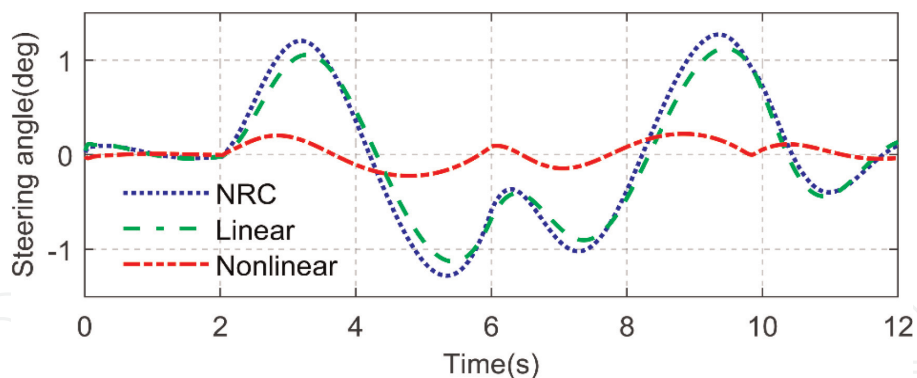


Figure 9.
 Steering angle of NRC under DLC scene.

4.2 Serpentine scene

Figures 10 and 11 illustrate the global trajectories and lateral errors during serpentine tracking. It can be observed that the NRC controller exhibits smaller maximum lateral errors compared to the LQR and RHC controllers. Furthermore, the NRC controller demonstrates higher response speed and superior transient performance in comparison with the other two controllers. These findings indicate that the NRC controller outperforms the LQR and RHC controllers in terms of tracking performance on serpentine roads.

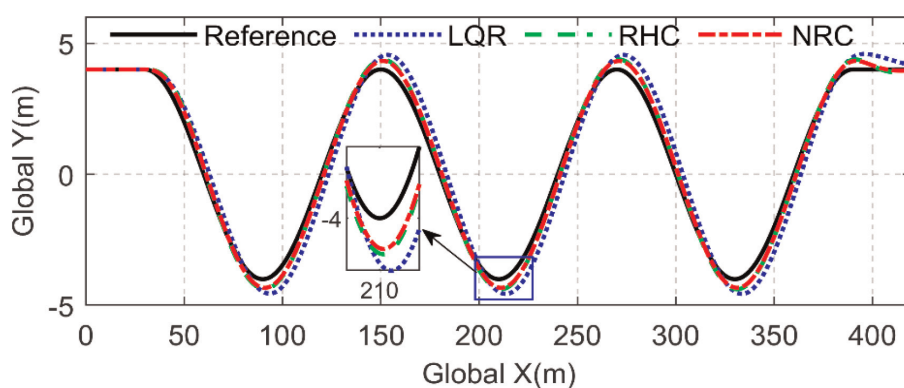


Figure 10.
 Global trajectories of three controllers under serpentine scene.

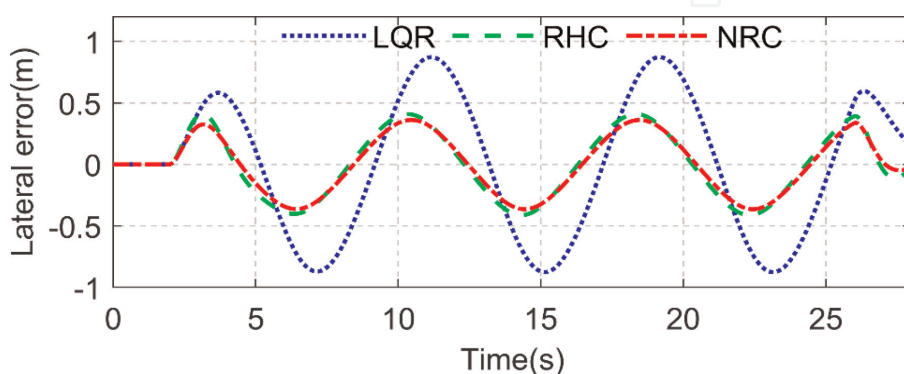


Figure 11.
 Lateral errors of three controllers under serpentine scene.

Figures 12 and 13 present the road curvature and front wheel angle of the serpentine scene. The maximum of serpentine road curvature is approximately $0.01(1/m)$. Similar to the DLC scene, the front wheel angle value of the NRC lies within the range of the LQR and RHC controllers. The inclusion of nonlinear compensation enables NRC to demonstrate stable trajectory-following capability.

In Figures 14 and 15, it can be observed that NRC responds quickly with minimal yaw error when tracking a trajectory with large curvature. This results in low yaw error and ensures stable tracking performance. Figure 16 illustrates the angle of linear and nonlinear feedback of NRC under the serpentine scene. The value of the nonlinear

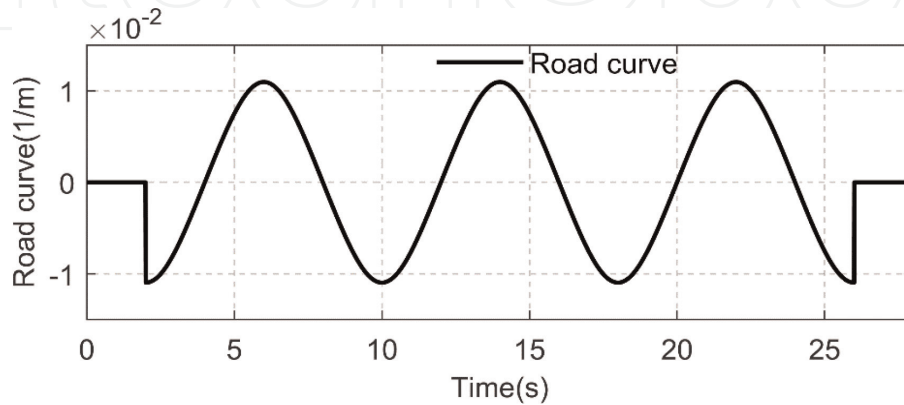


Figure 12.
Curvature of road under serpentine scene.

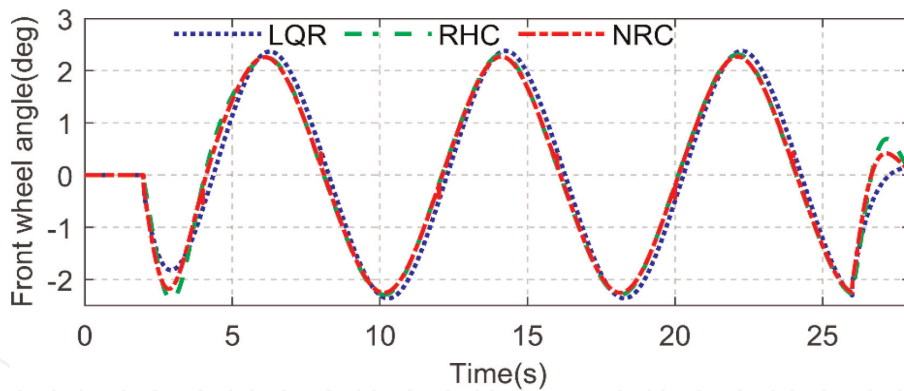


Figure 13.
Front wheel angle of three controllers under serpentine scene.

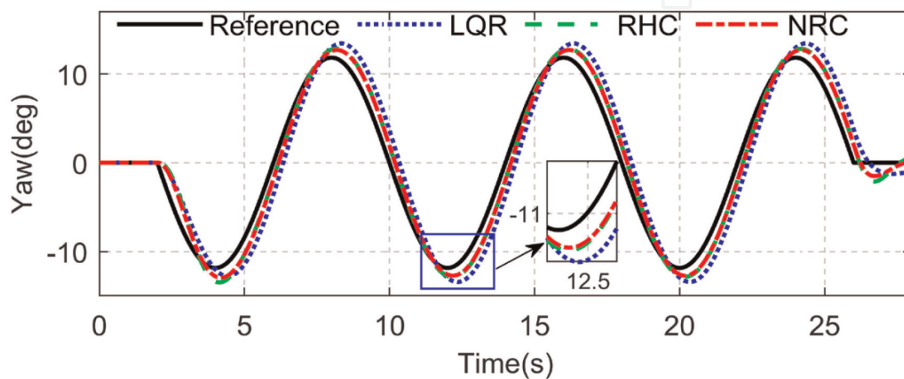


Figure 14.
Yaw of three controllers under serpentine scene.

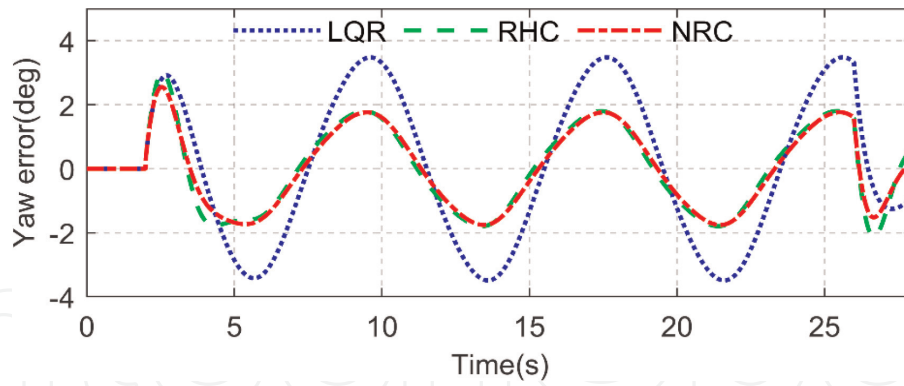


Figure 15.
 Yaw error of three controllers under serpentine scene.

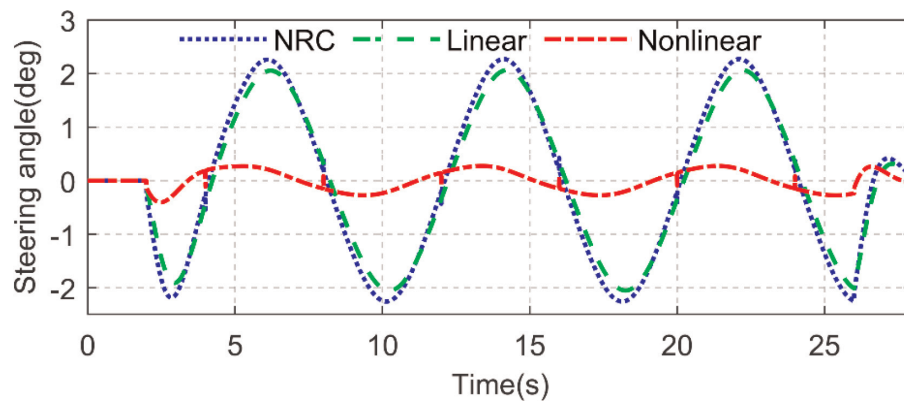


Figure 16.
 Steering angle of NRC under serpentine scene.

compensation function aligns with the trend of linear feedback, and it contributes to enhanced system response speed and trajectory tracking accuracy.

The mean absolute lateral error (MAE), maximum lateral error (ME), and root-mean-square lateral error (RMSE) are used to quantitatively analyze the trajectory-following performance of NRC, and the RHC and LQR controllers are utilized as comparative test.

Table 2 presents the values of ME, MAE, RMSE, RI, and RII for the lateral displacement in both DLC and serpentine scenes. The data clearly indicate NRC achieves smaller ME, MAE, and RMSE compared to LQR and RHC in both scenarios.

Scene	Index(y_e)	LQR(m)	RHC(m)	NRC(m)	RI	RII
DLC	ME	0.395	0.244	0.193	51.30%	20.96%
	MAE	0.178	0.102	0.087	51.12%	14.49%
	RMSE	0.220	0.131	0.108	50.95%	17.69%
Serpentine	ME	0.876	0.413	0.365	58.40%	11.64%
	MAE	0.472	0.224	0.196	58.36%	12.42%
	RMSE	0.552	0.264	0.232	57.94%	12.08%

Notes: $RI = (LQR - NRC)/LQR$, $RII = (RHC - NRC)/RHC$.

Table 2.
 Quantitatively analyze of lateral error under two scenes.

The larger errors observed in the DLC scene can be attributed to the significant lateral displacement in this scenario, which lead to greater trajectory-following errors. In terms of performance improvement, NRC demonstrates an overall enhancement of over 50% compared to LQR in the DLC scene, and over 57% improvement in the serpentine scene. Additionally, under the DLC scene, NRC exhibits a 20.96% higher ME than RHC, which indicates its faster system response in trajectory-following with large model state errors. Furthermore, the MAE of NRC is approximately 14.49% in the DLC scene, which is higher than RHC, it highlights its smaller errors compared to RHC. Overall, the proposed controller outperforms RHC and LQR by offering advantages such as fast response speed and reduced overshoot.

5. Conclusion

To enhance the precision of trajectory-following, speed of system response, and suppression of overshoot in the control system for AGEV equipped with AFS system, we propose a novel NRC strategy. Initially, we establish the system dynamics of AGEV and its vehicle trajectory-following control system with dynamic error. By applying Lyapunov stability theory, we ultimately design the nonlinear robust H -infinity controller for the AGEV trajectory-following system. The proposed controller is solved by using a set of linear matrix inequalities. The efficacy of the proposed controller is validated by utilizing MATLAB/Simulink and Carsim[®] software. The simulation results demonstrate that the proposed controller has efficient trajectory-following performance compared to RHC and LQR.

Conflict of interest

The authors declare no conflict of interest.

Author details


Xianjian Jin^{1,2*} and Qikang Wang¹

1 School of Mechatronic Engineering and Automation, Shanghai University, Shanghai, China

2 Shanghai Key Laboratory of Intelligent Manufacturing and Robotics, Shanghai University, Shanghai, China

*Address all correspondence to: jinxianjian@yeah.net

IntechOpen

© 2023 The Author(s). Licensee IntechOpen. This chapter is distributed under the terms of the Creative Commons Attribution License (<http://creativecommons.org/licenses/by/3.0>), which permits unrestricted use, distribution, and reproduction in any medium, provided the original work is properly cited. 

References

- [1] Deng H, Zhao Y, Nguyen AT, Huang C. Fault-tolerant predictive control with deep-reinforcement-learning-based torque distribution for four in-wheel motor drive electric vehicles. *IEEE/ASME Transactions on Mechatronics*. 2023; **28**(2):668-680. DOI: 10.1109/TMECH.2022.3233705
- [2] Yassine A, Hossain MS, Muhammad G, Guizani M. Double auction mechanisms for dynamic autonomous electric vehicles energy trading. *IEEE Transactions on Vehicular Technology*. 2019; **68**(8):7466-7476. DOI: 10.1109/TVT.2019.2920531
- [3] Barari A, Saraygord AS, Liang X. Coordinated control for path-following of an autonomous four in-wheel motor drive electric vehicle. *Proceedings of the Institution of Mechanical Engineers, Part C: Journal of Mechanical Engineering Science*. 2022; **236**(11):6335-6346. DOI: 10.1177/09544062211064797
- [4] Gözü M, Ozkan B, Emirler MT. Disturbance observer based active independent front steering control for improving vehicle yaw stability and tire utilization. *International Journal of Automotive Technology*. 2022; **23**(3): 841-854. DOI: 10.1007/s12239-022-0075-1
- [5] Mousavinejad E, Han QL, Yang F, Zhu Y, Vlacic L. Integrated control of ground vehicles dynamics via advanced terminal sliding mode control. *Vehicle System Dynamics*. 2017; **55**(2):268-294. DOI: 10.1080/00423114.2016.1256489
- [6] Wang Y, Nguyen B, Fujimoto H, Hori Y. Multirate estimation and control of body slip angle for electric vehicles based on onboard vision system. *IEEE Transactions on Industrial Electronics*. 2014; **61**:1133-1143. DOI: 10.1109/TIE.2013.2271596
- [7] Wang G, Liu Y, Li S, Tian Y, Zhang N, Cui G. New integrated vehicle stability control of active front steering and electronic stability control considering tire force reserve capability. *IEEE Transactions on Vehicular Technology*. 2021; **70**:2181-2195. DOI: 10.1109/TVT.2021.3056560
- [8] Cho J, Huh K. Active front steering for driver's steering comfort and vehicle driving stability. *International Journal of Automotive Technology*. 2019; **20**: 589-596. DOI: 10.1007/s12239-019-0056-1
- [9] Falcone P, Borrelli F, Asgari J, Tseng H, Hrovat D. Predictive active steering control for autonomous vehicle systems. *IEEE Transactions on Control Systems Technology*. 2007; **15**:566-580. DOI: 10.1109/TCST.2007.894653
- [10] Soltani A, Azadi S, Jazar RN. Integrated control of braking and steering systems to improve vehicle stability based on optimal wheel slip ratio estimation. *Journal of the Brazilian Society of Mechanical Sciences and Engineering*. 2022; **44**(3):102. DOI: 10.1007/s40430-022-03420-2
- [11] Hladio A, Nielsen C, Wang D. Path following for a class of mechanical systems. *IEEE Transactions on Control Systems Technology*. 2012; **21**(6): 2380-2390. DOI: 10.1109/TCST.2012.2223470
- [12] Ahmadian N, Khosravi A, Sarhadi P. Driver assistant yaw stability control via integration of AFS and DYC. *Vehicle system dynamics*. 2022; **60**(5): 1742-1762. DOI: 10.1080/00423114.2021.1879390

- [13] Ghaffari V. Optimal tuning of composite nonlinear feedback control in time-delay nonlinear systems. *Journal of the Franklin Institute*. 2020;**357**(2): 1331-1356. DOI: 10.1016/j.jfranklin.2019.12.024
- [14] Mobayen S. Robust tracking controller for multivariable delayed systems with input saturation via composite nonlinear feedback. *Nonlinear Dynamics*. 2014;**76**(1):827-838. DOI: 10.1007/s11071-013-1172-5
- [15] Yu S, Li X, Chen H, Allgöwer F. Nonlinear model predictive control for path following problems. *International Journal of Robust and Nonlinear Control*. 2015;**25**(8):1168-1182. DOI: 10.1002/rnc.3133
- [16] Chen J, Shuai Z, Zhang H, Zhao W. Path following control of autonomous four-wheel-independent-drive electric vehicles via second-order sliding mode and nonlinear disturbance observer techniques. *IEEE Transactions on Industrial Electronics*. 2020;**68**(3): 2460-2469. DOI: 10.1109/TIE.2020.2973879
- [17] Liu Z, Chen X, Yu J. Adaptive sliding mode security control for stochastic markov jump cyber-physical nonlinear systems subject to actuator failures and randomly occurring injection attacks. *IEEE Transactions on Industrial Informatics*. 2022;**19**(3):3155-3165. DOI: 10.1109/TII.2022.3181274
- [18] Zhao X, Liu Z, Jiang B, Gao C. Switched controller design for robotic manipulator via neural network-based sliding mode approach. *IEEE Transactions on Circuits and Systems II: Express Briefs*. 2023;**70**(2):561-565. DOI: 10.1109/TCSII.2022.3169475
- [19] Xu B, Sun F, Pan Y, Chen B. Disturbance observer based composite learning fuzzy control of nonlinear systems with unknown dead zone. *IEEE Transactions on Systems, Man, and Cybernetics: Systems*. 2016;**47**(8): 1854-1862. DOI: 10.1109/TSMC.2016.2562502
- [20] Cao H, Song X, Zhao S, Bao S, Huang Z. An optimal model-based trajectory-following architecture synthesising the lateral adaptive preview strategy and longitudinal velocity planning for highly automated vehicle. *Vehicle System Dynamics*. 2017;**55**(8): 1143-1188. DOI: 10.1080/00423114.2017.1305114
- [21] Cervantes J, Yu W, Salazar S, Chairez I. Takagi-Sugeno dynamic neuro-fuzzy controller of uncertain nonlinear systems. *IEEE Transactions on Fuzzy Systems*. 2016;**25**(6):1601-1615. DOI: 10.1109/TFUZZ.2016.2612697
- [22] Wu Y, Wang L, Zhang J, Li F. Path following control of autonomous ground vehicle based on nonsingular terminal sliding mode and active disturbance rejection control. *IEEE Transactions on Vehicular Technology*. 2019;**68**(7): 6379-6390. DOI: 10.1109/TVT.2019.2916982
- [23] Ding T, Zhang Y, Ma G, Cao Z, Zhao X, Tao B. Trajectory tracking of redundantly actuated mobile robot by MPC velocity control under steering strategy constraint. *Mechatronics*. 2022;**84**:102779. DOI: 10.1016/j.mechatronics.2022.102779
- [24] Moradi H, Vossoughi G, Movahhedy MR, Salarieh H. Suppression of nonlinear regenerative chatter in milling process via robust optimal control. *Journal of Process Control*. 2013;**23**(5):631-648. DOI: 10.1016/j.jprocont.2013.02.006
- [25] Fu Y, Li B, Fu J. Multi-model adaptive switching control of a nonlinear

system and its applications in a smelting process of fused magnesia. *Journal of Process Control*. 2022;115:67-76.
DOI: 10.1016/j.jprocont.2022.04.009

[26] Fahmy SFF, Banks SP. Robust H -infinity control of uncertain nonlinear dynamical systems via linear time-varying approximations. *Nonlinear Analysis: Theory, Methods & Applications*. 2005;63(5-7):2315-2327.
DOI: 10.1016/j.na.2005.03.030

[27] Ju G, Wu Y, Sun W. Adaptive output feedback asymptotic stabilization of nonholonomic systems with uncertainties. *Nonlinear Analysis: Theory, Methods and Applications*. 2009;71(11):5106-5117. DOI: 10.1016/j.na.2009.03.088

[28] Li SE, Gao F, Li K, Wang LY, You K, Cao D. Robust longitudinal control of multi-vehicle systems-a distributed H -infinity method. *IEEE Transactions on Intelligent Transportation Systems*. 2017;19(9):2779-2788. DOI: 10.1109/TITS.2017.2760910